Single-passage NMRON investigation of ^{125}Sb impurities in single-crystal iron

1991 J. Phys.: Condens. Matter 3 467

(http://iopscience.iop.org/0953-8984/3/4/010)

J. Phys.: Condens. Matter 3 (1991) 467–482. Printed in the UK

Single-passage NMRON investigation of ^{125}Sb impurities in single-crystal iron

N Yazidjoglou, W D Hutchison and G A Stewart
Department of Physics, University College, The University of New South Wales, Australian Defence Force Academy, Campbell, ACT 2600, Australia

Received 27 June 1990, in final form 24 October 1990

Abstract. Single-passage NMRON results for dilute ^{125}Sb in single-crystal Fe, have been acquired as a function of RF power for various applied DC fields along the [100] 'easy' axis and quantitatively analysed. This is the first time that such data have been described in terms of an absolute theory without the benefit of arbitrary ordinate scaling factors. The introduction of a simple model to account for the observed dependence of the RF skin depth on applied DC field is shown to be successful in two ways. Firstly it enables the determination of the relaxation constant, C_K = 1.0 s K (0 T), 2.25 s K (0.3 T), 3.0 s K (0.45 T) and 3.25 s K (0.6 T), and secondly it permits sensible estimates of the adiabatic parameter at the surface, A_S, to be deduced.

1. Introduction

In the continuing study of dilute impurities in cubic ferromagnetic hosts, the relaxation constant, C_K, associated with the spin–lattice relaxation (SLR) of impurity nuclei is an important experimental parameter against which hyperfine (HF) interaction models can be tested. Nuclear orientation (NO) based techniques are particularly suitable for the determination of C_K because they are applicable to systems sufficiently dilute that impurity–impurity interactions can be ignored. However, it is necessary to know the nuclear sublevel populations just prior to SLR. For this reason, non-resonant NO methods such as thermal cycling (Klein 1977) and fast cooling (Barclay *et al* 1972) have been considered the most reliable. In each case, the populations prior to SLR are described by a single elevated Boltzmann temperature which can be determined experimentally.

In principle, resonant NO techniques should also be straightforward to apply to the determination of C_K. That is, it should be possible to use a resonant radio frequency (RF) signal to perturb the nuclear sublevel populations and then monitor the subsequent SLR. After all, for the case of a discrete, pure magnetic dipole HF interaction, the effect of any RF perturbation can be described in terms of a nuclear 'ensemble rotation' (Stewart *et al* 1977) through some angle which can be determined experimentally. In practice however, there are three complicating factors.

(i) Inhomogeneous broadening. The strength of the dominant magnetic dipole HF interaction varies from impurity site to impurity site, resulting in an approximately Gaussian distribution of resonance frequencies about the central frequency, f_0. The half-width at half maximum, Γ_{HWHM}, of the distribution is much larger than the intrinsic

0953-8984/91/040467 + 16 $03.50

resonance width. Hence, a substantial perturbation of the sublevel populations is achieved only if the effective RF strength, f_1, is large compared with Γ_{HWHM} and/or the RF frequency, f, is modulated.

(ii) Quadrupole perturbation. The impurity nuclei experience an additional small electric quadrupole HF interaction (Callaghan *et al* 1974a) even if the substitutional sites have cubic crystallographic symmetry. For techniques where the quadrupole perturbation cannot be ignored, the simple ensemble rotation concept is rendered invalid.

(iii) RF skin effect. RF energy is lost to the metallic specimen via the process of Joule heating. Therefore the RF strength decays exponentially according to

$$f_1(x) = f_{1S} \exp(-x/\delta) \tag{1}$$

where x is the penetration depth, δ is the so-called RF skin depth and f_{1S} represents the effective RF strength at the specimen's surface. Unless the root mean square depth, x_{RMS}, of impurity impregnation into the specimen is much smaller than δ, the nuclei experience a distribution of RF strengths.

The principal resonant NO technique employed in this work is single passage NMRON (NMR on oriented nuclei), while single-pulse NMRON is used to assist in characterization of the RF skin effect. Each technique is subject to two of the above three complicating factors. The consequence is that the sublevel populations just prior to SLR are no longer described by a single parameter which can be determined unambiguously from the experimental data. Instead, key parameters of unknown value must be varied systematically until theoretical curves match the data.

Single-pulse NMRON applies single, resonant RF pulses with a field strength much greater than the quadrupole perturbation, so the ensemble rotation concept holds. However, nuclei located in different parts of the distribution experience ensemble rotations through different angles which depend, in turn, on the local RF field strength. The key parameters (Isbister and Chaplin 1990) which must be adjusted to fit the immediate post-pulse data are then

$$R = f_{1S}/\Gamma_{HWHM} \tag{2}$$

$$w = x_{RMS}/\delta \tag{3}$$

and

$$\beta_0 = 2\pi f_{1S}\tau \tag{4}$$

where τ is the duration of the pulse.

The single-passage NMRON technique can be considered as a special case of frequency-modulated NMRON. As the name suggests, it involves a single sweep of the RF frequency either 'up' from below the inhomogeneously broadened line to above it or 'down' from above the line to below it. In the case of a pure magnetic dipole HF interaction, the nuclei experience an ensemble rotation through an angle which depends only on the local adiabatic parameter,

$$A = 2\pi f_1^2/(\mathrm{d}f/\mathrm{d}t) \tag{5}$$

and is independent of the direction of the sweep. It was for this reason that single-passage NMRON was initially envisaged as the resonant NO technique most suitable for C_K determination. Since the discovery of the small quadrupole perturbation, exploitation of single-passage NMRON for this purpose has been largely abandoned. Initial attempts

at fitting theoretical curves to single-passage responses were directed at determining the magnitude of the quadrupole perturbation (Callaghan *et al* 1975, 1976a, 1976b). Although the importance of the RF skin effect was recognised, it was dealt with by introducing an arbitrary scaling factor. Also, since a population transformation theory was not available for intermediate values of A, an empirical function with the correct asymptotic behaviour was adopted. However, the theory for single-passage NMRON on a quadrupole-perturbed system is now well established and it is straightforward to average over the exponential A distribution brought about by the RF skin effect. The key parameters become the adiabatic parameter at the specimen surface, A_S, the skin depth ratio, w (equation (3)) and the relaxation constant C_K.

The primary aim of this work is to demonstrate that current theory can be fitted reliably to experimental single-passage NMRON curves (i.e. single-passage plus SLR), especially when the curves are considered in conjunction with single-pulse NMRON data recorded for the same specimen. To this end, a series of single-passage NMRON data curves for single-crystal ^{125}SbFe has been chosen for detailed analysis. This specimen offers a large working radiation anisotropy and the strength of the negative quadrupole perturbation has already been measured (Chaplin *et al* 1988) using MAPON (modulated adiabatic passage on ON), a recently developed, spectroscopic extension of the single-passage NMRON technique. Hence the fitted values of A_S and w can be tested against the conditions under which the theory is expected to hold. Furthermore, Sb lies towards the heavy impurity end of the 4d–5p series of probes where the agreement between experimental and theoretical estimates of C_K appears to break down (Klein 1986). The values of C_K determined in this work will be compared with earlier experimental results.

2. Theory

Figure 1 shows a simplified scheme for the decay of ^{125}Sb to ^{125}Te. When ^{125}Sb is present as a substitutional impurity in the ferromagnetic iron host, the hyperfine splitting of the $I = \frac{7}{2}$ parent state is dominated by the magnetic dipole interaction. The normalized angular distribution of gamma radiation emitted for subsequent nuclear transitions is then given (Krane 1986) by

$$W(\theta) = 1 + B_2U_2A_2P_2(\theta) + B_4U_4A_4P_4(\theta) \tag{6}$$

where θ is the angle between the direction of detection and the local magnetic field at the nuclei. A small external DC field, $\boldsymbol{B}_{app}$, is applied to force all magnetic domains (and hence all local fields) into alignment. Where this is not achieved, the Legendre polynomials, $P_\nu(\theta)$, must be replaced by their weighted averages over the distribution of θ-values. The U_ν parameters describe the reorientation effect of intermediate transitions and the A_ν parameters are angular momentum coupling coefficients for the observed decay. The B_ν coefficients provide the link with the nuclear sublevel populations, p_m, of the parent state which, at thermal equilibrium, depend on the Zeeman splitting and the lattice temperature via the Boltzmann distribution. The central resonance frequency is given by

$$f_0 = \mu_{7/2}\mu_N B_0/hI \tag{7}$$

where

$$\boldsymbol{B}_0 = \boldsymbol{B}_{HF} + \boldsymbol{B}_{app} - \mu_0 D\boldsymbol{M}. \tag{8}$$

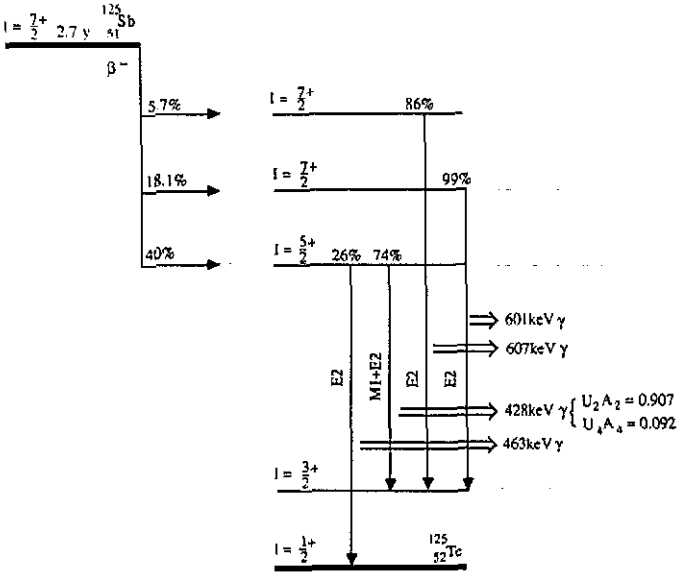

Figure 1. Partial ^{125}Sb decay scheme showing the four gamma transitions monitored. $U_\nu A_\nu$ coefficient products (Krane *et al* 1971) are included only for the 428 keV γ-transition which has been used for all NMRON experiments in the present work.

$\boldsymbol{B}_{\mathrm{HF}}$ is the HF field, $\boldsymbol{M}$ is the bulk electronic magnetization and D is the demagnetizing factor.

The electric quadrupole perturbation

$$\delta E_m = P[m^2 - \tfrac{1}{3}I(I+1)] \tag{9}$$

is too small to influence the equilibrium populations but can be large compared with the RF strength. This work will assume that the condition

$$2P/h \gg f_1 \tag{10}$$

holds at all times. The theory for a single passage through any homogeneous packet of nuclei then reduces to a sequence of independent two-level subresonances (figure 2). A subresonance involving the states $|m\rangle$ and $|m+1\rangle$ can be treated as a spin $I' = \frac{1}{2}$ system (Callaghan *et al* 1974a) with an effective adiabatic parameter, A'_m, given by

$$A'_m = [I(I+1) - m(m+1)]A \tag{11}$$

where A is the true adiabatic parameter defined in equation (5). Straightforward application of the ensemble rotation theory (Stewart *et al* 1977) then yields

$$p_m(\text{final}) = (1 - f_m)p_m(\text{initial}) + f_m p_{m+1}(\text{initial}) \tag{12a}$$

$$p_{m+1}(\text{final}) = f_m p_m(\text{initial}) + (1 - f_m)p_{m+1}(\text{initial}) \tag{12b}$$

where

$$f_m = 1 - \exp(-\pi A'_m/2) \tag{13}$$

is a measure of the degree of population inversion for the $m \leftrightarrow m+1$ subresonance.

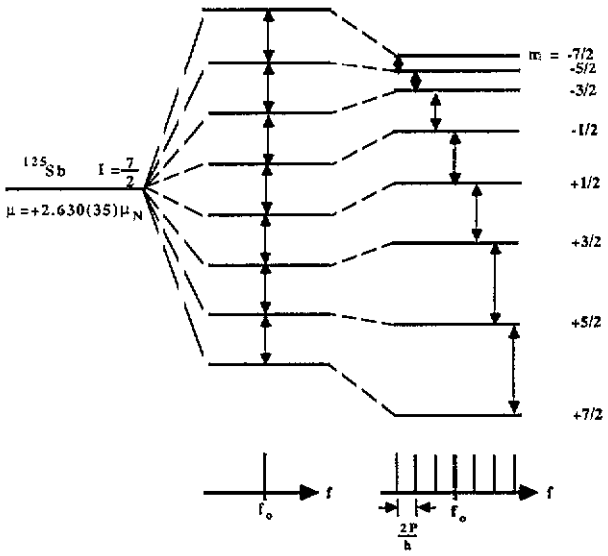

Figure 2. Exaggerated schematic representation of the influence of a discrete, negative ($P < 0$), quadrupole perturbation on ^{125}Sb nuclei at the centre of the inhomogeneously broadened resonance line.

Unlike the pure magnetic dipole HF interaction case, the combined effect of a single passage through all $2I$ quadrupole-split subresonances is sweep direction dependent.

Following Klein (1986), the SLR curve is obtained by numerical Runge–Kutta solution of the master equation

$$\frac{\mathrm{d}p_m}{\mathrm{d}t} = \sum_n (W_{n\to m}p_n - W_{m\to n}p_m) \tag{14}$$

with transition probabilities

$$W_{m\to m+1} = W_{m+1\to m}\,\mathrm{e}^{T_{\mathrm{int}}/T} = (T_{\mathrm{int}}/2C_{\mathrm{K}})[I(I+1) - m(m+1)]/(1 - \mathrm{e}^{-T_{\mathrm{int}}/T}) \tag{15}$$

where $T_{\mathrm{int}} = hf_0/k_{\mathrm{B}}$. If necessary (i.e. if the RF sweep is sufficiently slow), SLR can be included between successive subresonances. Because the total quadrupole splitting for any homogeneous spin packet is small compared with the inhomogeneous line broadening, any structure in the mid-passage response is smeared out after convolution with the Guassian line shape.

The influence of the RF skin effect is included by performing a weighted average over single-passage curves computed for different A-values. In this work, the ^{125}Sb activity is diffused into the surface of a slice of single-crystal iron and it is assumed that the impurity concentration decreases exponentially with depth according to

$$c(x) = c_{\mathrm{S}} \exp(-x\sqrt{2}/x_{\mathrm{RMS}}). \tag{16}$$

The adiabatic parameter is proportional to f_1^2 which also decreases exponentially with penetration depth (equation (1)). RF field inhomogeneities due to the coil geometry and

Table 1. Theoretical estimates of $w = x_{RMS}/\delta$ for the ^{125}SbFe specimen. Although the quoted μ_r values are those most commonly employed in the NMRON literature, it is now believed that they are inappropriate (see section 3).

μ_r	σ $(10^8\,(\Omega\,m)^{-1})$	δ (μm)	w	
			$x_{RMS} = 5.3\,\mu m$[a]	$x_{RMS} = 1.4\,\mu m$[b]
200[c]	26.7[e]	0.06	88	23
($B_{app} = 0$)	3.3[f]	0.17	31	8
1[d]	26.7[e]	0.85	6.2	1.6
(saturation)	3.3[f]	2.4	2.2	0.6

[a,b] x_{RMS} estimates using diffusion constants of $D_0 = 0.11\,m^2\,s^{-1}$ (Bruggeman and Roberts 1968) and $0.008\,m^2\,s^{-1}$ (Myers and Rack 1978) respectively.
[c] Gray (1972).
[d] Johnson and Rado (1949).
[e] Fulkerson *et al* (1966).
[f] White (1968).

specimen surface quality are assumed to be negligible by comparison. Hence the single-passage curve for surface adiabatic parameter, A_S, is given by

$$\overline{W(A_S; t)} = \int_0^\infty e^{-\xi\sqrt{2}} W(A = A_S e^{-2\xi w}; t)\,d\xi \Big/ \int_0^\infty e^{-\xi\sqrt{2}}\,d\xi \tag{17}$$

where ξ is the dimensionless variable x/x_{RMS} and w is the skin depth ratio already defined in equation (3). In practice, convoluted single-passage curves are computed for selected adiabatic parameters and in interpolation procedure is employed for the evaluation of the integrals in equation (17).

3. Proposed RF skin depth model

It should be possible to derive a theoretical estimate of the skin depth ratio, w, rather than treat it as a variable parameter. x_{RMS} can be calculated using Ficks' laws and the RF skin depth is given by

$$\delta = (\pi f \mu_r \mu_0 \sigma)^{-1/2} \tag{18}$$

where σ is the electrical conductivity of the iron host and μ_r is the relative permeability. However, as demonstrated in table 1, the resultant w estimate depends very much on which published diffusion constants and electrical conductivities are adopted. Moreover, despite the fact that they are commonly employed in the NMRON literature, it is believed that the polycrystalline specimen μ_r values quoted in table 1 are inappropriate for the present single-crystal geometry. The low field ($B_{app} = 0$) polycrystalline value of $\mu_r = 200$ is determined mainly by domain wall displacement and the saturation value of $\mu_r = 1$ is for B_{RF} applied parallel to B_{app} so that domain wall rotation plays only a minimal role. By contrast, in the present work, B_{RF} is applied perpendicularly to B_{app} which is directed along the easy [100] axis in the surface of a well-oriented, single-crystal disc. Hence it is expected that domain rotation will dominate the permeability within the impurity diffusion layer close to the specimen's surface. A simple model, similar to the

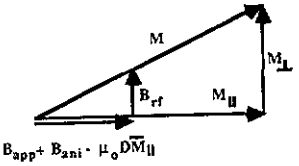

Figure 3. Vector geometry employed for the proposed skin depth model.

RF enhancement model, is therefore proposed for the derivation of the perpendicular relative permeability component, $\mu_r^\perp$. If the electronic magnetization is assumed to follow the total effective field acting upon it, then it is evident from figure 3 that

$$M_\perp/B_{RF} = M_\parallel/(B_{app} + B_{ani} - \mu_0 D\bar{M}_\parallel) \tag{19}$$

where B_{ani} is the anisotropy field. $M_\parallel$ and $\bar{M}_\parallel$ are the parallel components of the local domain magnetization and the bulk magnetization respectively. Perpendicular contributions to the demagnetizing field can be ignored because $M_\perp$ is induced only within the thin skin depth layer of the specimen and the demagnetizing factor will be negligible. Using $\mu_r^\perp = 1 + \chi_\perp$ and $\chi_\perp = \mu_0 M_\perp/B_{RF}$, equation (19) gives

$$\mu_r^\perp \approx 1 + [\mu_0 M/(B_{app} + B_{ani} - \mu_0 D\bar{M}_\parallel)] \tag{20}$$

where it has been assumed that $M_\parallel \approx M$. For the [100] easy axis of single crystal iron, the low temperature magnetic anisotropy coefficient (Danan *et al* 1968, Escudier 1973) corresponds to $B_{ani} = 0.064$ T. Therefore, for $B_{app} = 0$ and $\bar{M}_\parallel \approx 0$ (no magnetic prehistory), equation (20) yields $\mu_r^\perp \approx 36$ compared with the zero-DC-field value of $\mu_r = 200$ quoted in table 1. The model predicts, via equation (18), that the RF skin depth will increase with increased B_{app}. Consequently, the skin depth ratio, w, will decrease with increased B_{app}. The approach taken in this work is to determine the w value for $B_{app} = 0$ and then scale this value according to equation (20) for the cases with non-zero DC field.

4. Experimental details

The ^{125}SbFe specimen was prepared by diffusing ~164 μCi of ^{125}Sb carrier free activity into a 1 mm thick, 10 mm diameter, Fe single crystal cut along the (110) plane. At first the crystal was mechanically polished (down to 0.05 μm alumina paste) until the surface was clear of observable scratches as seen via a ×40 optical microscope. Then the ^{125}Sb radioactivity was electroplated (70 h at 2.7 V DC and ~0.5 mA) to a 3 mm diameter area of the polished surface using a platinum anode in the radioactive solution. Finally, the specimen was annealed for 10 min at 850 °C under an atmosphere of H_2 followed by a 7 h cool to room temperature. Excess activity was wiped from the surface with ethanol. For this heat treatment, Ficks' laws give root mean square diffusion depths of x_{RMS} = 5.3 μm or 1.4 μm depending on which published diffusion constant is used (see table 1). The corresponding surface ^{125}Sb concentrations are 0.033 at.% and 0.125 at.% respectively.

The single-crystal specimen was soldered to the copper cold finger of a dilution refrigerator with $\boldsymbol{B}_{app}$ and the γ-detection directed along the surface [100] direction as previously identified by Laue back diffraction. A pair of 12 mm diameter loops of copper wire generated $\boldsymbol{B}_{RF}$ perpendicular to the applied field and parallel to the sample surface. Temperatures of ~10 mK were achieved for all NMRON measurements and the RF input

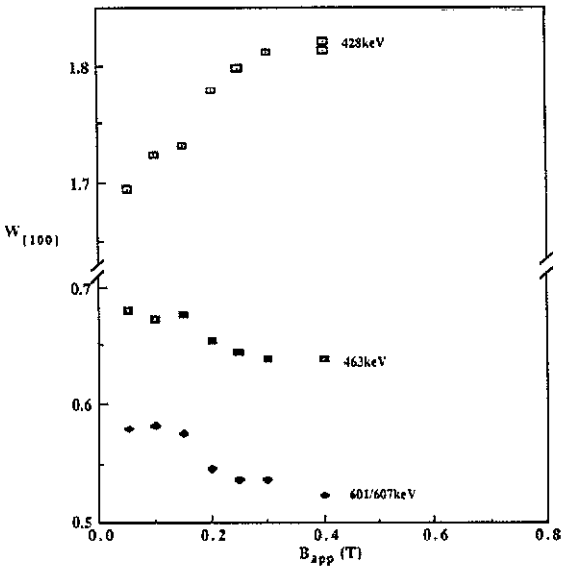

Figure 4. Magnetization curves for single-crystal ^{125}SbFe with $B_{app}\|[100]$. The 428 keV, 463 keV and 601 keV/607 keV γ-transitions were monitored in pulse height analysis mode for a lattice temperature of ≈7 mK.

was gated to ensure minimal non-resonant heating. The RF level was monitored by disconnecting the cable from the cryostat input and recording the peak-to-peak voltage, V_{RF}, across a 50 Ω, room temperature termination. For the single-pulse NMRON experiments, a 4 kW amplifier capable of V_{RF} = 1600 V (at 130 MHz) was used.

Pulses from the high purity germanium detector were fed into a multi-channel analyser with multi-tasking capability. NMRON responses were recorded in multi-channel scaling mode using pulses from a single-channel analyser window set about the 428 keV photopeak. A ^{54}MnNi NO thermometer was continuously monitored in pulse height analysis mode to give the specimen temperature. This temperature was used to adjust the window counts to give the true anisotropy values.

5. Experimental results and analysis

Magnetization curves for the 428 keV, 463 keV and 601/607 keV γ-transitions are shown in figure 4. The large anisotropies obtained at $B_{app} \sim 0.05$ T verify that the ^{125}SbFe specimen was correctly aligned along the 'easy' [100] axis and it is evident that the crystal magnetization is saturated at $B_{app} \geq 0.3$ T. The 428 keV transition was selected to monitor all subsequent NMRON experiments, because its gamma anisotropy is approximately twice that of the other two transitions, and because its gamma anisotropy is positive (increased count rate).

5.1. The resonances

Resonance line shapes were established by stepping through the frequency and recording γ-counts for both frequency modulation on and frequency modulation off (conventional

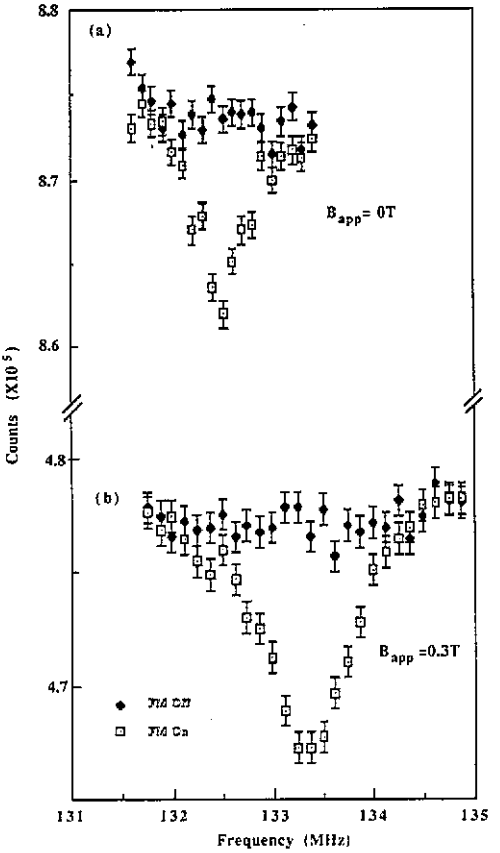

Figure 5. Representative resonance lineshapes for single-crystal ^{125}SbFe with $V_{RF} = 0.89$ V and $B_{app}\|[100]$. Respective frequency modulation amplitudes (warm counts) are (*a*) 100 kHz (738800) and (*b*) 250 kHz (302500).

CW NMRON). Figure 5 shows representative line shapes recorded for $B_{app} = 0$ T and $B_{app} = 0.3$ T. The large increase in line width for the 0.3 T resonance is not a result of the larger frequency modulation amplitude employed (±125 kHz compared with ±50 kHz for $B_{app} = 0$ T) but represents a true increase in inhomogeneous broadening arising from random demagnetizing fields at the specimen surface. The frequency modulation contribution to the apparent line width is expected to be less than 2% of the true line width. Experimental Γ_{HWHM} and f_0 values for the low DC field region ($B_{app} \leq 0.6$ T) relevant to subsequent single-passage measurements are summarized in table 2. f_0 is also shown in figure 6 as a function of B_{app}. Assuming zero Knight shift, the gradient of the linear portion of the full line yields a magnetic moment of $|\mu_{7/2}| = 2.630(3)\ \mu_N$ compared with the accepted value of $\mu_{7/2} = +2.630(35)\ \mu_N$ (Langouche *et al* 1977, Callaghan *et al* 1974b). The broken line included in figure 6 shows the frequency shift expected for a thin foil specimen. The horizontal displacement of the two lines gives the saturation value of the bulk demagnetizing field for the single-crystal specimen as $\mu_0 D M_{sat} = 0.13$ T. An identical theoretical estimate is obtained by treating the disk as an ellipsoid with $D = 0.0615$ (Osborn 1945) and assuming $M_{sat} = 2.216\ \mu_B$/Fe site (Danan *et al* 1968).

5.2. Zero-field single-pulse NMRON

Single, resonant, RF pulses (132.5 MHz, 1200 V_{PP}) were applied repeatedly to the specimen with $B_{app} = 0$ T and sufficient time allowed between pulses for the nuclear ensemble

Table 2. Resonance and single-passage NMRON details for ^{125}SbFe with $B_{app}\|[100]$. The A_S, w and C_K parameters are those used for the theoretical curves in figures 8 and 9.

B_{app} (T)	f_0 (MHz)	Γ_{HWHM} (kHz)	V_{RF} (V)	$V_{RF}^2\Delta t$ (V^2 s)	Non-resonant heating	A_S	$\mu_r^{\perp}$ [b]	w	C_K (s K)
0.00	132.5	300	10	125	Large				
			5.0	31.3	Significant				
			2.5	10.6	Negligible	0.75	36	7.0	1.0
			1.3	2.9	Zero	0.30	36	7.0	1.0
			0.6	0.45	Zero	0.11	36	7.0	1.0
0.05	132.5	240							
0.15	132.6[a]		5.0	31.3	Significant				
0.30	133.4	480	5.0	31.3	Negligible	0.25	10	3.7[c]	2.25
0.45	134.3	≈500	5.0	31.3	Zero	0.18	7	3.1[c]	3.0
0.60	135.2[a]		5.0	31.3	Zero	0.18	5	2.9[c]	3.25

[a] Interpolated from figure 6.
[b] Calculated using equation (20) with $B_{int} = 0.064$ T and $\mu_0 DM_{sat} = 0.13$ T.
[c] Derived from $w(B_{app} = 0) = 7.0$ assuming $w \propto (\mu_r^{\perp} f_0)^{1/2}$.

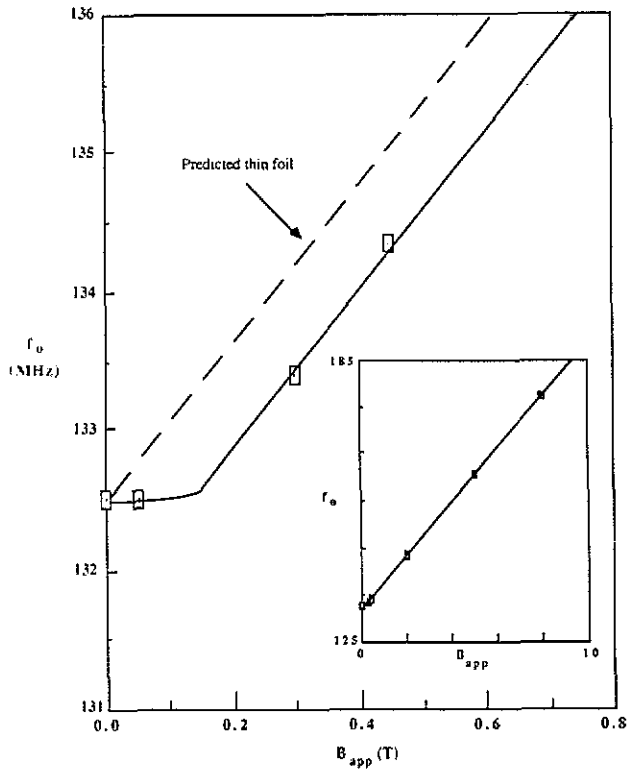

Figure 6. Central resonance frequency for ^{125}SbFe as a function of $B_{app}\|[100]$. The high field data (inset) have been discussed elsewhere (Yazidjoglou *et al* 1988). The broken line indicates the frequency shift expected for a thin specimen with negligible demagnetizing field.

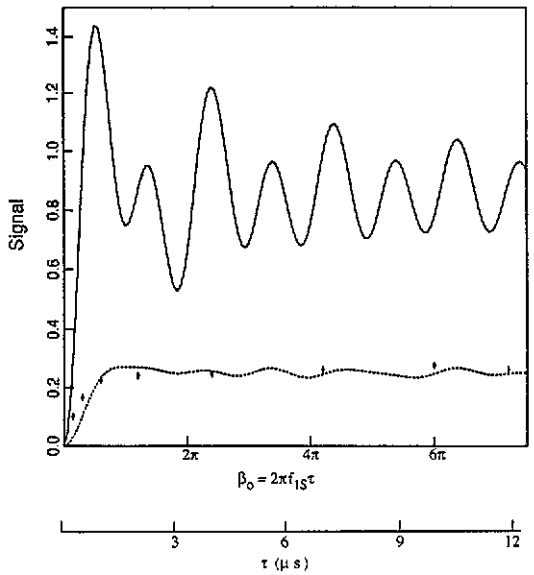

Figure 7. ^{125}SbFe single-pulse NMRON signal (fractional destruction of γ anisotropy) as a function of pulse duration, τ, with $V_{RF} = 1200$ V, and $B_{app} = 0$ T. The theoretical curves are for $R = 1$, $w = 0$ (full curve) and $R = 1$, $w = 7$ (broken line).

to relax back to equilibrium. The average, immediate post-pulse signals are shown in figure 7 for pulses of duration $\tau = 0.25, 0.5, 1, 2, 4, 7, 10$ and 12 μs. The experimental signal is seen to rise to a low, featureless plateau as τ is increased. Such behaviour is symptomatic of a strong RF skin effect (Isbister and Chaplin 1990). Only the skin depth ratio, w, is required for the single-passage NMRON theory and, once R is assigned, w is determined precisely by the plateau signal. However, because of the absence of signal maxima and minima (such as occur for $w = 0$), the assignment of R is not so clear cut. An alternative approach is to consider the location of the plateau's 'knee' below which the signal drops away. From the work of Isbister and Chaplin, the plateau acquires a marked slope for $R > 2$ and, for $R \leqslant 2$, the 'knee' is located at $\beta_0 = 100 \pm 10°$. The 'knee' of the experimental data falls in the range $0.75\ \mu s \leqslant \tau \leqslant 1.0\ \mu s$ implying that $f_{IS} = 326 \pm 90$ kHz. Given that $\Gamma_{HWHM} \approx 300$ kHz for $B_{app} = 0$ T (from section 5.1), then $R = 1.1 \pm 0.3$. For the purpose of the present analysis, it has been assumed that $R = 1$, corresponding to $f_{IS} = 300$ kHz. It is on the basis of this f_{IS} determination that the experimental signals have been assigned their β_0 values. The broken curve in figure 7 gives the theoretical signal as a function of $\beta_0 = 2\pi f_{IS}\tau$ with $R = 1$ and a best fit value of $w = 7$. For consistency, it has been recalculated (Isbister 1990) for an exponential impurity profile rather than a step profile as adopted by Isbister and Chaplin. The theoretical curve for $R = 1$ and $w = 0$ (solid curve) has been included for comparison to demonstrate the influence of the skin effect.

5.3. Single-passage NMRON

The single-passage NMRON data were recorded with 1.5 MHz sweeps through the resonance line in sweep times of either $\Delta t = 1.25$ s or $\Delta t = 1.7$ s. Figure 8 shows pairs

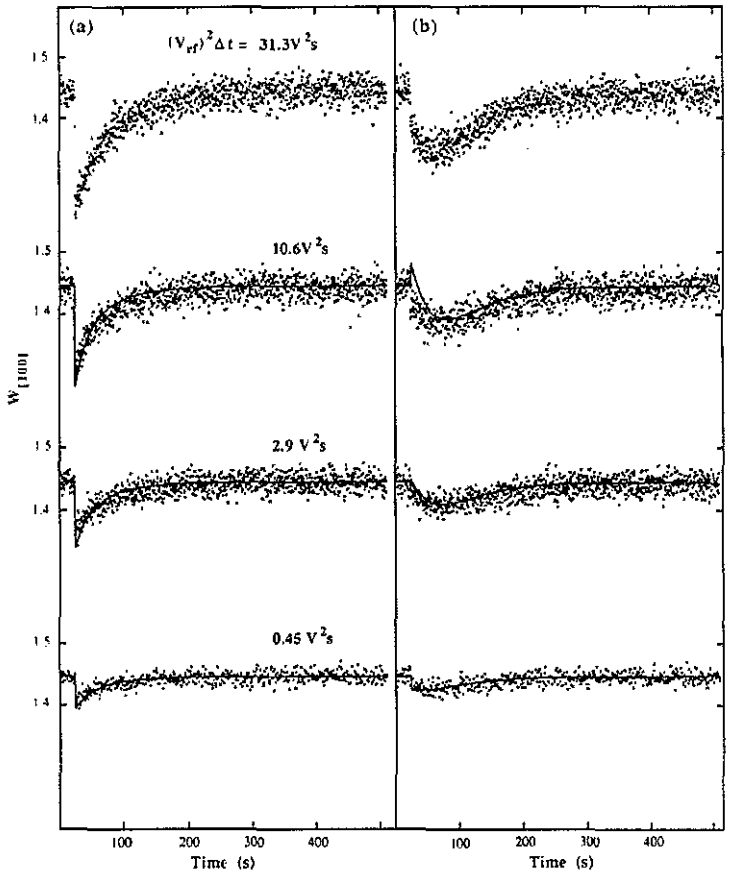

Figure 8. Zero-field ^{125}Sb**Fe** single-pasage NMRON responses as a function of $(V_{RF})^2\Delta t$ for (a) sweep 'up' and (b) sweep 'down'. *The simulated curves (full curves) were computed for* $P_{|100|}/h = -7$ kHz (Chaplin *et al* 1988) and parameters as detailed in table 2. Due to significant non-resonant heating (see figure (10*d*)), a theoretical fit was not attempted for $(V_{RF})^2\Delta t = 31.3\ V^2\,s$.

(sweep 'up'/sweep 'down') of experimental single-passage curves as a function of $V_{RF}^2\Delta t$ for $B_{app} = 0$ T. A strong sweep direction dependence is observed for $V_{RF}^2\Delta t = 31.3\ V^2$ s and persists down to $V_{RF}^2\Delta t = 0.45\ V^2$ s where the RF perturbation is considerably smaller. The SLR for sweep 'up' ('down') is compatible with the RF having entered the least (most) populated quadrupole split subresonances first and corresponds to a negative quadrupole perturbation ($P_{|100|} < 0$) as assumed in figure 2. The magnitude of $P_{|100|}/h$ has been determined elsewhere as |7.0(8)| kHz, using MAPON spectroscopy (Chaplin *et al* 1988). Figure 9 shows pairs of single passages as a function of B_{app} for constant $V_{RF}^2\Delta t = 31.3\ V^2$ s. Note that the time taken for the nuclear ensemble to relax back to thermal equilibrium increases with B_{app}. This is particularly evident for the sweep 'down' curves. Off-resonance single passages were performed to investigate the influence of the non-resonant RF heating (figure 10). With $B_{app} = 0$ T, the non-resonant heating is negligible for $V_{RF}^2\Delta t \leqslant 10.6\ V^2$ s (figure 10(*e*)) but cannot be ignored for $V_{RF}^2\Delta t \geqslant 31.3\ V^2$ s (figure 10(*d*)). However, the non-resonant heating for

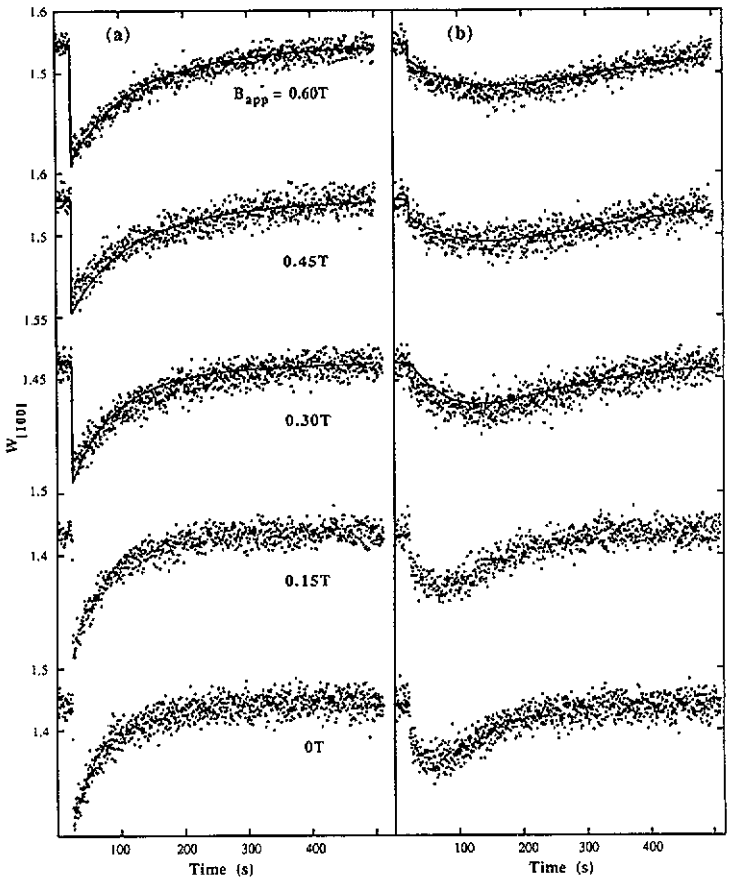

Figure 9. ^{125}SbFe single-passage NMRON responses as a function of applied field for (a) sweep 'up' and (b) sweep 'down'. $(V_{RF})^2\Delta t$ is constant at 31.3 V^2 s. The simulated curves (full curves) were computed for $P_{|100|}/h = -7$ kHz (Chaplin *et al* 1988) and parameters as detailed in table 2. Theoretical fits were not attempted for $B_{app} = 0$ T (see figure 10(*d*) for evidence of significant non-resonant heating) and $B_{app} = 0.15$ T (unknown domain alignment).

$V_{RF}^2\Delta t = 31.3\ V^2$ s decreases with DC applied field (figure 10(*a*)–(*d*)) and becomes negligible for $B_{app} \geqslant 0.30$ T. This can be explained in terms of the skin effect model. As the DC applied field is increased, the RF skin depth increases and less heating occurs in the surface layer monitored by ^{125}Sb probes. The first six columns of table 2 summarize the experimental details for all single-passage NMRON experiments.

The full curves in figures 8 and 9 are theoretical curves fitted to those single-passage data where the non-resonant heating can be ignored. It was found that each experimental single-passage response could be simulated exactly if all three parameters (A_S, w and C_K) were free to vary. However, in order to force sensible results, the parameters were constrained to give:

(i) identical A_S and C_K for sweep 'up' and sweep 'down';

(ii) identical w and C_K for the same B_{app};

(iii) $w \propto \sqrt{(\mu_r^{\perp} f_0)}$ according to the proposed skin depth model (section 3) with $w = 7$ for $B_{app} = 0$ T as determined from the single-pulse NMRON measurements.

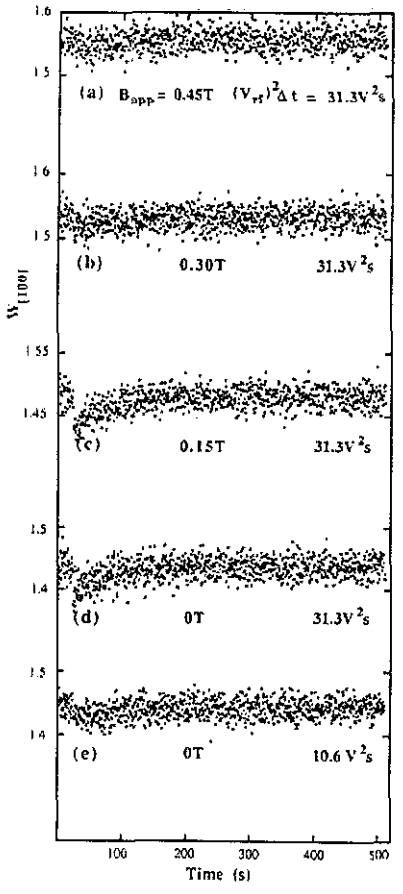

Figure 10. Off-resonance single-passage NMRON responses used to monitor the extent of non-resonant RF heating.

Since the RF strength at the probe nuclei is notoriously difficult to calibrate in NMRON experiments, A_S was retained as an independent parameter from one sweep 'up'/sweep 'down' pair to another. For the data for zero DC field, it was assumed that the majority fraction, F, of domains align with the [100] easy axis in the plane of the specimen's surface while remaining domains align with the [100] axes perpendicular to this direction. Hence for the theory calculations, the $P_\nu(0°)$ in equation (6) were replaced by $FP_\nu(0°) + (1 - F)P_\nu(90°)$. The thermal equilibrium data for $B_{app} = 0$ T corresponded to $F \approx 92.5\%$. For $B_{app} \geq 0.3$ T, it was assumed that the bulk magnetization was saturated. The f_{1S} value determined for the single-pulse NMRON was scaled to the lower RF voltages employed for single-passage NMRON and used to derive starting estimates of the surface adiabatic parameters, A_S. It was found that the locations, with respect to time, of the half-maximum perturbation for the sweep 'up' SLR and the broad minimum for the sweep 'down' SLR could be used to determine how the value of C_K should be adjusted. The approach was then to compute pairs of theoretical curves as a function of A_S for a selection of C_K. The A_S and C_K thus judged to give the best 'eye-fit' are included in table 2 together with the values of w.

6. Discussion and conclusion

The most significant general point to emerge from the NMRON data analysis undertaken

in the current investigation is that the RF skin depth cannot be ignored. Both the single-pulse NMRON signal and the reduction of non-resonant heating with increased DC applied field provide direct experimental evidence for this. The x_{RMS} diffusion depth was estimated to be 1.4 μm–5.3 μm (table 1) for the present single-crystal specimen. Therefore to reduce the experimentally determined skin depth ratio from $w = 7$ to $w < 1$ would require an x_{RMS} of order 0.1 μm–0.5 μm. This dimension is small even when compared with thicknesses of polycrystalline foil specimens where the tendency is to ignore the RF skin effect. The situation worsens for frequencies higher than 130 MHz.

In this report the RF skin effect was tackled quantitatively via the proposed skin depth model, which proved successful in two ways. First, its implicit field dependence enabled w values at $B_{app} \geqslant 0.3$ T to be calculated from the value determined experimentally at $B_{app} = 0$ T, without resorting to dubious theoretical calculations of x_{RMS} and δ. This semi-empirical approach eliminated the skin depth ratio, w, as a parameter to be fitted to the single-passage NMRON curves. Second, the model predicted a much less dramatic fall in w with increasing B_{app} than implied by the values of $\mu_r = 200$ ($B_{app} = 0$ T) and $\mu_r = 1$ (saturation) traditionally quoted in the NMRON literature, while merely assuming no DC applied field dependence of the conductivity. This enabled the curves recorded at $B_{app} = 0.45$ T and $B_{app} = 0.6$ T to be described with a surface adiabatic parameter large enough that sweep direction dependence was preserved. According to equation (5), the adiabatic parameter is expected to be proportional to the product $V_{RF}^2 \Delta t$. From table 2, $A_S(B_{app} = 0\,\text{T})$ follows this trend although the proportionality is not strictly adhered to. Similarly, A_S decreases with increased B_{app} but the field dependence is not as strong as that predicted by the enhancement model ($A_S \propto [1 + B_{HF}/(B_{app} + B_{ani} - \mu_0 DM)]^2$). It should be stressed that no scaling factor has been introduced.

The suitability of adiabatic parameter values determined can be observed by considering the maximum adiabatic parameter fitted to the single-passage NMRON data; $A_S = 0.75$ for $B_{app} = 0$ T with $V_{RF} = 2.5$ V (table 2). This corresponds to a maximum effective RF strength of $f_{1S} = 0.32$ kHz. By comparison, the single-pulse calibration of $f_{1S} = 300$ kHz ($R = 1$) for $V_{RF} = 1200$ V scales to give $f_{1S} = 0.63$ kHz for $V_{RF} = 2.5$ V. Furthermore, the maximum $f_{1S} = 0.32$ kHz is considerably smaller than $2|P_{[100]}|/h = 14$ kHz so that equation (10) holds and the analysis is consistent with the single-passage NMRON theory as described in section 2. From table 2, the resultant C_K are seen to increase with applied field to give a saturation value of $C_{K\infty}[100] \approx 3.25$ s K. This trend is now well established for impurity SLR (Klein 1986) and it is commonly understood that the current theoretical models describe the high field limit. However, the *ab initio* calculations presented by Klein (1986) predict a value of $C_K \approx 7.7$ s K for Sb**Fe**. The present experimental results compare more favourably with the earlier results of C_K ($B_{app} \approx 0.2$ T) = 2.8 s K (Reid *et al* 1967) and C_K (B_{app} unknown) = 3.2 s K (Barclay *et al* 1968) as recalculated by Klein (1986) for polycrystalline foil specimens. Since the latter result represents a simple exponential fit to the SLR following frequency modulation across the resonance line, it is evident that the present work's attempt to more correctly define the sublevel populations prior to SLR has had little influence on the experimental value of $C_{K\infty}$. The disparity between experiment and theory remains.

In conclusion, this work has demonstrated that a series of single-passage NMRON curves can be analysed theoretically but only if allowances are made for a strong RF skin effect. The C_K relaxation constants thus obtained do not significantly modify earlier results and hence support the evidence for disagreement between experiment and theory towards the end of the 4d–5p series of impurity probes in the iron host.

Acknowledgments

The authors acknowledge the assistance of both Assoc. Professor D H Chaplin and Dr M Kopp and wish to thank Dr D J Isbister for his recalculation of the single-pulse NMRON signal for an exponential diffusion profile. This work was supported by a grant from the Australian Research Council. The authors also wish to acknowledge the constructive comments of a referee.

References

Barclay J A, Brewer W D, Matthias E and Shirley D A 1968 *Hyperfine Structure and Nuclear Radiations* ed D A Shirley and E Matthias (Amsterdam: North Holland) p 902
Barclay J A, Chaplin D H, Don C G and Wilson G V H 1972 *Phys. Rev.* B **6** 2565
Bruggeman G and Roberts J 1968 *J. Metall.* **20** 54
Callaghan P T, Johnston P D, Lattimer W M and Stone N J 1975 *Phys. Rev.* B **12** 3526
Callaghan P T, Johnston P D and Stone N J 1974a *J. Phys. C: Solid State Phys.* **7** 3161
Callaghan P T, Lattimer W M, Johnston P D and Stone N J 1976a *Hyperfine Interact.* **2** 288
Callaghan P T, Lattimer W M and Stone N J 1976b *Hyperfine Interact.* **2** 291
Callaghan P T, Shott M and Stone N J 1974b *Nucl. Phys.* A **221** 1
Chaplin D H, Hutchison W D, Kopp M and Yazidjoglou N 1988 *Hyperfine Interact.* **43** 241
Danan H, Herr A and Meyer A J P 1968 *J. Appl. Phys.* **39** 669
Escudier P 1973 *PhD Thesis* University of Grenoble
Fulkerson W, Moore J P and McElroy D L 1966 *J. Appl. Phys.* **37** 2639
Gray D E (ed) 1972 *American Institute of Physics Handbook* (New York: McGraw-Hill)
Isbister D J 1990 private communication
Isbister D J and Chaplin D H 1990 *Z. Naturf.* a **45** 43
Johnson M H and Rado G T 1949 *Phys. Rev.* **75** 841
Klein E 1977 *Hyperfine Interact.* **3** 389
—— 1986 *Low Temperature Nuclear Orientation* ed N J Stone and H Postma (Amsterdam: North Holland) ch 12
Krane K S 1986 *Low Temperature Nuclear Orientation* ed N J Stone and H Postma (Amsterdam: North Holland) Appendix 5
Krane K S, Sites J R and Steyert W A 1971 *Phys. Rev.* C **4** 565
Langouche G, Triplett B B, Dixon N S, Hanna S S and Boolchand P 1977 *Phys. Rev.* C **15** 1043
Myers S M and Rack H J 1978 *J. Appl. Phys.* **49** 3246
Osborn J A 1945 *Phys. Rev.* **67** 351
Reid P G E, Sott M and Stone N J 1967 *Phys. Lett.* **25A** 456
Stewart G A, Barclay J A, Don C G, Lester L N and Wilson G V H 1977 *Phys. Rev.* C **10** 3651
White G K 1968 *Experimental Techniques in Low Temperature Physics* 2nd edn (Oxford: Oxford University Press)
Yazidjoglou N, Chaplin D H, Fopster H R and Hutchison W D 1988 *Hyperfine Interact.* **43** 231